Structure of Si(114) determined by global optimization methods

F. C. Chuang[1], C. V. Ciobanu[2]* C. Predescu[3], C. Z. Wang[1], and K. M. Ho[1]

[1]Ames Laboratory – U.S. Department of Energy and
Department of Physics, Iowa State University, Ames, Iowa 50011, USA

[2]Division of Engineering, Colorado School of Mines, Golden, Colorado 80401, USA

[3]Department of Chemistry and Kenneth S. Pitzer Center for
Theoretical Chemistry, University of California, Berkeley, CA 94720, USA

Abstract

In this article we report the results of global structural optimization of the Si(114) surface, which is a stable high-index orientation of silicon. We use two independent procedures recently developed for the determination of surface reconstructions, the parallel-tempering Monte Carlo method and the genetic algorithm. These procedures, coupled with the use of a highly-optimized interatomic potential for silicon, lead to finding a set of possible models for Si(114), whose energies are recalculated with ab-initio density functional methods. The most stable structure obtained here without experimental input coincides with the structure determined from scanning tunneling microscopy experiments and density functional calculations by Erwin, Baski and Whitman [Phys. Rev. Lett. 77, 687 (1996)].

*Corresponding author. Email: cciobanu@mines.edu, Phone: 303-384-2119, Fax: 303-273-3602

1   Introduction

While the low-index semiconductor surfaces have dominated the interest of surface scientists for several decades, at present a considerable amount of work is being dedicated to high-index orientations. Since the high-index surfaces exhibit more diverse structural and electronic properties, the adept use of these properties can constitute the key for various technological applications, in particular for the fabrication of devices at length scales where lithographic techniques are not applicable. Controlling certain physical processes (e.g., growth of nanostructures in a preferred direction) depends in part on having knowledge of the structure of the substrate surface. The main technique for investigating atomic-scale features of surfaces is scanning tunelling microscopy (STM), although STM alone is only able to provide "a range of speculative structural models which are increasingly regarded as solved surface structures" [1]. A common procedure for finding the reconstructions of silicon surfaces consists in a combination of STM imaging and density functional calculations as follows. Starting from the bulk truncated surface and taking cues from the experimental data, one proposes several atomic models for the surface reconstructions. These models are then relaxed using electronic structure methods; at the end of relaxation, surface energies and STM images are *computed* for each structural model. A match with the experimental STM data is identified based on the relaxed lowest-energy structures and their simulated STM images (e.g., [2, 3, 5]). As described, the procedure is heuristic, as one needs to rely heavily on physical intuition when proposing good candidates for the lowest energy reconstructions of high-index surfaces.

Treating the reconstruction of semiconductor surfaces as a problem of global optimization, we have recently developed a parallel tempering Monte Carlo procedure for studying the structure and thermodynamics of crystal surfaces [6], as well as a genetic algorithm for structure determination [7]. The use of such methods can help avoid situations in which the actual physical reconstruction of a high-index surface is not part of the set of heuristic models that are considered for computation of surface energies and comparison with experimental data. Given that there are examples of semiconductor surfaces (e.g., [3, 4]) for which the initially proposed models did not withstand further scientific scrutiny from different research groups, it appears worthwhile to perform searches for the structure of some of stable high-index surface orientations of silicon. One such surface is Si(114), reported to be as stable as the well studied low-index surfaces Si(001) and Si(111) [5]: given this stability of Si(114), it is somewhat surprising that this surface has not attracted more interest, at least from a technological perspective. There are few studies of Si(114) to date, which include the pioneering study reporting on the atomic configuration [5], and two recent works reporting on the electronic structure of this surface [18].

Based on scanning tunelling microscope (STM) images combined with density functional calculations, two atomic models [(2×1) and $c(c \times 2)$], were proposed for the Si(114) orientation [5]. These models have very similar bonding topology, differing only in terms of dimerization pattern of their surface. The surface energies of the two models are also similar, as both can be found on sufficiently large areas of the scanned samples [5]. To our knowledge, so far Ref.

[5] represents the *only* proposal for the structure of Si(114). The purpose of this article is to present several other model candidates for the structure of Si(114), models that are likely to be experimentally observed on this surface. Addressing the problem of atomic structure from a different perspective than the previous reports [5, 18], we perform stochastic searches for the global minimum configuration of this surface. As we shall see, the lowest energy configuration (at zero Kelvin) obtained here from purely theoretical means is consistent with the original proposal [5]; however, the global search methods provide several other structural models with low surface energy, which could be relevant in various experimental conditions. The remainder of this paper is organized as follows. Section II presents the two recently developed global search algorithms, the parallel tempering Monte Carlo methods and the genetic algorithm for structure determination. While brief descriptions of these methods are provided in Sec. II, we refer the reader to our recent works [6, 7] for full details related to their implementation. The results of the structural optimization for Si(114) surface are presented and discussed in Section III, and our conclusions are outlined in the last section.

2 Methods

2.1 Parallel-tempering Monte Carlo method

The reconstructions of semiconductor surfaces are determined not only by the efficient bonding of the surface atoms, but also by the stress created in the process [3]. Therefore, we retain a large number of subsurface atoms when performing a global search for the lowest energy configuration: this way the surface stress is intrinsically considered when reconstructions are sorted out. The number of local minima of the potential energy is also large, as it scales roughly exponentially [8, 9] with the number of atoms involved in the reconstruction; by itself, such scaling requires the use of fast stochastic search methods. One such method is the parallel-tempering Monte Carlo (PTMC) algorithm [10, 11], which was shown to successfully find the reconstructions of a vicinal Si surface when coupled with an exponential cooling [6]. Before outlining the procedure, we discuss briefly the computational cell and the empirical potential used.

The simulation cell (of dimensions $3a \times a\sqrt{2}$ in the plane of the surface) has a single-face slab geometry with periodic boundary conditions applied in the plane of the surface, and no periodicity in the direction normal to it. The "hot" atoms from the top part of the slab (10–15 Å thick) are allowed to move, while the bottom layers of atoms are kept fixed to simulate the underlying bulk crystal. The area of the simulation cell and the number of atoms in the cell are kept fixed during each simulation. Under these conditions, the problem of finding the most stable reconstruction reduces to the global minimization of the total potential energy $V(\mathbf{x})$ of the atoms in the simulation cell (here $\mathbf{x}$ denotes the set of atomic positions). In terms of atomic interactions, we are constrained to use empirical potentials because the highly accurate ab-initio or tight-binding methods are prohibitive as far as the search itself is concerned. Since this work is aimed at finding the *lowest* energy reconstructions for arbitrary surfaces, the

choice of the empirical potential is important. After numerical experimentation with several empirical models, we chose to use the highly optimized empirical potential (HOEP) recently developed by Lenosky *et al.* [12]. HOEP is fitted to a large database of ab-initio calculations using the force-matching method, and provides a good description of the energetics of all atomic coordinations up to $Z = 12$.

The parallel tempering Monte Carlo method (also known as the replica-exchange Monte-Carlo method) consists in running parallel canonical simulations of many statistically independent replicas of the system, each at a different temperature $T_1 < T_2 < \ldots < T_N$. The set of N temperatures $\{T_i, \ i = 1, 2, ..., N\}$ is called a temperature schedule (or schedule for short). The probability distributions of the individual replicas are sampled with the Metropolis algorithm [13], although any other ergodic strategy can be employed [14]. Irrespective of what sampling strategy is being used for each replica, the key feature of the parallel tempering method is that swaps between replicas of neighboring temperatures T_i and T_j $(j = i \pm 1)$ are proposed and allowed with the conditional probability [10, 11] given by

$$\min \left\{ 1, e^{(1/T_j - 1/T_i)[V(\mathbf{x}_j) - V(\mathbf{x}_i)]/k_B} \right\} , \tag{1}$$

where $V(\mathbf{x}_i)$ represents the energy of the replica i and k_B is the Boltzmann constant. The conditional probability (1) ensures that the detailed balance condition is satisfied and that the equilibrium distributions are the Boltzmann ones for each temperature.

In the limit of low temperatures, the PTMC procedure allows for a geometric temperature schedule [15, 16]. To show this, we note that when the temperature drops to zero, the system is well approximated by a multidimensional harmonic oscillator, so the acceptance probability for swaps attempted between two replicas with temperatures $T < T'$ is given by the incomplete beta function law [16]

$$Ac(T, T') \simeq \frac{2}{B(d/2, d/2)} \int_0^{1/(1+R)} \theta^{d/2-1} (1 - \theta)^{d/2-1} d\theta , \tag{2}$$

where d denotes the number of degrees of freedom of the system, B is the Euler beta function, and $R \equiv T'/T$. Since it depends only on the temperature ratio R, the acceptance probability (2) has the same value for any arbitrary replica running at a temperature T_i, provided that its neighboring upper temperature T_{i+1} is given by $T_{i+1} = RT_i$. The value of R is determined such that the acceptance probability given by Eq. (2) attains a prescribed value p. Thus, the (optimal) schedule that ensures a constant probability p for swaps between neighboring temperatures is a geometric progression:

$$T_i = R^{i-1} T_{min}, \quad 1 \leq i \leq N, \tag{3}$$

where $T_{min} = T_1$ is the minimum temperature of the schedule.

The typical Monte Carlo simulation done in this work consists of two main parts that are equal in terms of computational effort. In the first stage of the computation, we perform

a parallel tempering run for a range of temperatures $[T_{min}, \; T_{max}]$. The configurations of minimum energy are retained for each replica, and used as starting configurations for the second part of the simulation, in which replicas are cooled down exponentially until the largest temperature drops below a prescribed value. As a key feature of the procedure, the parallel tempering swaps are not turned off during the cooling steps. Thus, in the second part of the simulation we are in fact using a combination of parallel tempering and simulated annealing, rather than a simple cooling. At the k-th cooling step, each temperature from the initial temperature schedule $\{T_i, i = 1, 2, ..., N\}$ is decreased by a factor which is independent of the index i of the replica, $T_i^{(k)} = \alpha_k T_i^{(k-1)}$. Because the parallel tempering swaps are not turned off, we require that at any cooling step k all N temperatures must be modified by the same factor α_k in order to preserve the original swap acceptance probabilities. We have used a cooling schedule of the form [6]

$$T_i^{(k)} = \alpha T_i^{(k-1)} = \alpha^{k-1} T_i \quad (k \geq 1), \tag{4}$$

where $T_i \equiv T_i^{(1)}$ and $\alpha = 0.85$.

The third and final part of the minimization procedure is a conjugate-gradient optimization of the last configurations attained by each replica. The relaxation is necessary because we aim to classify the reconstructions in a way that does not depend on temperature, so we compute the surface energy at zero Kelvin for the relaxed slabs i, $i = 1, 2, ..., N$. The surface energy γ is defined as the excess energy (with respect to the ideal bulk configuration) introduced by the presence of the surface:

$$\gamma = (E_m - n_m e_b)/A \tag{5}$$

where E_m is the potential energy of the n_m atoms that are allowed to move, $e_b = -4.6124\text{eV}$ is the bulk cohesion energy given by HOEP, and A is the surface area of the slab.

At the end of the simulation, we analyze the energies of the relaxed replicas. Typical plots showing the surface energies of the structures retrieved by the PTMC replicas are shown in Fig. 1(a), for different numbers of particles in the computational cell. To exhaust all the possibilities for the numbers of particles corresponding to the supercell dimensions of $3a \times a\sqrt{2}$, we repeat the PTMC simulation for different values of n ranging from 208 to 220, and look for a periodic behavior of the lowest surface energy as a function of n. For the case of Si(114), this periodicity occurs at intervals of $\Delta n = 4$, as shown in Fig. 1(b). Therefore, the (correct) number of atoms n at which the lowest surface energy is attained is $n = 216$, up to an integer multiple of Δn. As we shall show in the next section, the repetition of the simulation for different values of n in the simulation cell can be avoided within a genetic algorithm approach.

2.2 Genetic Algorithm

Like the previous method, the genetic algorithm also circumvents the intuitive process when proposing candidate models for a given high-index surface. An advantage of this algorithm
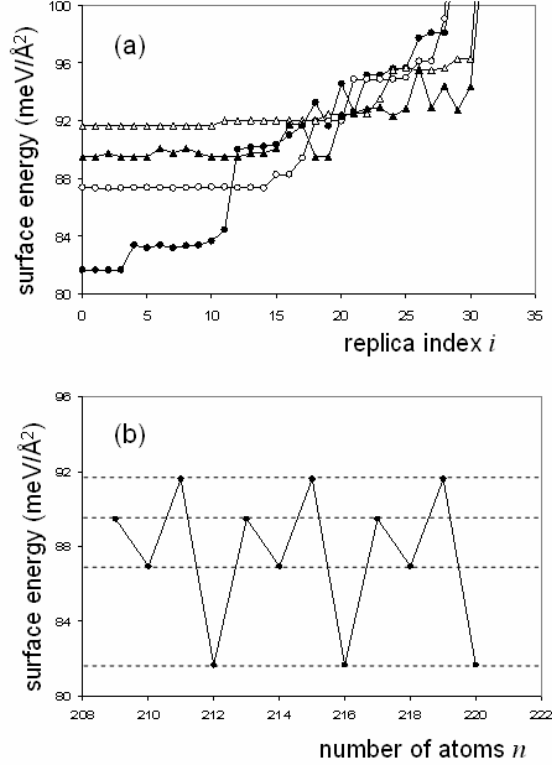
Figure 1: (a) Surface energies of the relaxed parallel tempering replicas i, $(0 \leq i \leq 31)$ with total number of atoms $n = 216$ (solid circles), 215 (open triangles), 214 (open circles) and 213 (solid triangles). For clarity, the range of plotted surface energies was limited from above at $100 \ \text{meV/Å}^2$. (b) Surface energy of the global minimum structure showing a periodic behavior as a function of n, with a period of $\Delta n = 4$; this finding helps narrowing down the set of values for n that need to be considered for determining the Si(114) reconstructions that have a $3a \times a\sqrt{2}$ periodic cell.

over most of the previous methodologies used for structural optimization is that the number of atoms involved in the reconstruction, as well as their most favorable bonding topology, can be found within the same genetic search. The development of a genetic algorithm (GA) for surface structure determination was motivated by its successful application for the structural optimization of atomic clusters [19, 20].

This search procedure is based on the idea of evolutionary approach in which the members of a generation (pool of models for the surface) mate with the goal of producing the best specimens, i.e. lowest energy reconstructions. "Generation zero" is a pool of p different structures obtained by randomizing the positions of the topmost atoms (thickness d), and by subsequently relaxing the simulation slabs through a conjugate-gradient procedure. The evolution from a generation to the next one takes place by mating, which is achieved by subjecting two randomly picked structures from the pool to a certain operation (mating) $\mathcal{O}$:(A,B)$\longrightarrow$C. The mating operation $\mathcal{O}$ produces a child structure C from two parent configurations A and B, as follows. The topmost parts of the parent models A and B (thickness d) are separated from the underlying bulk and sectioned by an arbitrary plane perpendicular to the surface. The (upper part of the) child structure C is created by combining the part of A that lies to the left of the cutting plane and the part of slab B lying to the right of that plane: the assembly is placed on a thicker slab, and the resulting structure C is subsequently relaxed.

A mechanism for the survival of the fittest is implemented as a defining feature of the genetic evolution. In each generation, a number of m mating operations are performed. The resulting m children are relaxed and considered for the possible inclusion in the pool based on their surface energy. If there exists at least one candidate in the pool that has a higher surface energy than that of the child considered, then the child structure is included in the pool. Upon inclusion of the child, the structure with the highest surface energy is discarded in order to preserve the total population p. As described, the algorithm favors the crowding of the ecology with identical metastable configurations, which slows down the evolution towards the global minimum. To avoid the duplication of members, we retain a new structure only if its surface energy differs by more than δ when compared to the surface energy of any of the current members p of the pool. Relevant values for the parameters of the algorithm are given in [7]: $10 \leq p \leq 40$, $m = 10$, $d = 5$Å , and $\delta = 10^{-5}$meV/Å^2.

We have developed two versions of the algorithm. In the first version, the number of atoms n is kept the same for every member of the pool by automatically rejecting child structures that have different numbers of atoms from their parents (mutants). In the second version of the algorithm, this restriction is not enforced, i.e. mutants are allowed to be part of the pool: in this case, the procedure is able to select the correct number of atoms for the ground state reconstruction without any increase over the computational effort required for one single constant-n run. The results of a variable-n run are shown in Fig. 2(a) which shows how the lowest energy and the average energy from a pool of $p = 30$ structures decreases as the genetic algorithm run proceeds. The plot in Fig. 2(a) displays typical features of the evolutionary approach: the most unfavorable structures are eliminated from the pool rather
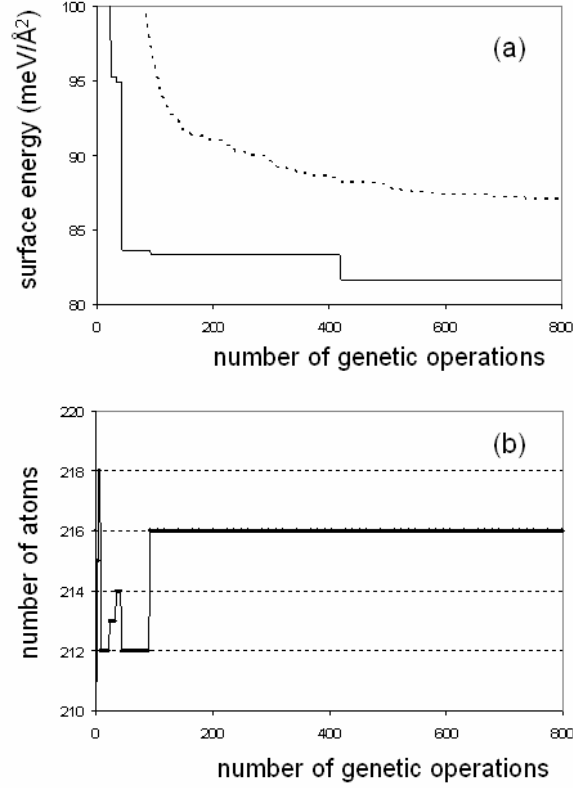
7

Figure 2: (a) Evolution of the lowest surface energy (solid line) and the average energy (dash line) for a pool of $p = 30$ structures during a genetic algorithm (GA) run with variable n ($210 \leq n \leq 222$). (b) Evolution of the number of atoms n that corresponds to the model with the lowest energy from the pool, during the same GA run. Note that the lowest energy structure of the pool spends most of its evolution in states with numbers of atoms that are compatible with the global minimum, i.e. $n = 212$ and $n = 216$.

fast (initial steep transient region of the graphs) and a longer time is taken for the algorithm to retrieve the most stable configuration. The lowest energy structure is retrieved in less than 500 mating operations. The correct number of atoms [refer to Fig. 2(b)] is retrieved much faster, within approximately 100 operations. It is worth noting that even during the transient period, the lowest-energy member of the pool spends most of its evolution in a state with a number of atoms ($n = 212$) that is compatible with the global minimum structure.

The two independent algorithms (PTMC and GA) presented briefly in this section are able to retrieve a set of possible candidates for the lowest energy surface structure. We use both of the algorithms in this work in order to assess how robust their structure predictions are. As it turns out, the two methods not only find the same lowest energy structures for each value of the total number of atoms n, but also most of the other low-energy reconstructions – a finding that builds confidence in the quality of the configuration sampling performed here. Since the atomic interactions are modelled by an empirical potential [12], it is desirable to check the relative stability of different model structures using higher-level calculations based on density functional theory; the details of these calculations are presented next.

2.3 Density functional calculations

Using the methodologies described above, we build a database of model structures that are sorted according to the surface energy given by the HOEP [12] interaction model. Since the empirical potentials may not give a reliable energetic ordering when a large number of structures are considered, we recalculate the surface energies of the models in the database at the level of density functional theory. The calculations where performed with the plane-wave based PWscf package [21], using the Perdew-Zunger [22] exchange-correlation energy. The slab geometry and the computational parameters are similar to the ones reported in [5]; given the increase in computational speed over the last eight years, we used thicker slabs and a different sampling of the Brillouin zone. The cutoff for the plane-wave energy was set to 12 Ry, and the irreducible Brilloiun zone was sampled with 4 k points. The equilibrium bulk lattice constant was determined to be $a = 5.41$Å, which was used for all the surface calculations in this work. The simulation cell has the single-face slab geometry, with 24 layers of Si, and a vacuum thickness of 12 Å. The bottom three layers are kept fixed in order to simulate the underlying bulk geometry, and the lowest layer is passivated with hydrogen. The remaining Si layers are allowed to relax until the forces become smaller than 0.025 eV/Å.

The surface energy γ for each reconstruction is determined indirectly, by first considering the surface energy γ_0 of an unrelaxed bulk truncated slab, then by calculating the difference $\Delta\gamma = \gamma - \gamma_0$ between the surface energy of the actual reconstruction and the surface energy of bulk truncated slab that has the bottom three layers fixed and hydrogenated. The energy of the bulk truncated surface, as computed from a two-faced slab with 24 layers, was found to be $\gamma_0 = 143$ meV/Å^2. This indirect procedure for calculating the surface energies at the DFT level was outlined, for instance, in Ref. [2].

9

3 Structural models for Si(114)

At the end of the global search procedures, we obtain a set of model structures which we sort by the number of atoms in the simulation cell and by their surface energy. Since the empirical potentials may not be fully transferable to different surface environments, we study not only the global minima given by the model for different values of n, but also most of the local minima that are within 15 meV/Å^2 from the lowest energy configurations. After the global optimizations, the structures obtained are also relaxed by density functional theory (DFT) methods as described in Sec. 2.3. The results are summarized in Table 1, which will be discussed next.

3.1 Results

Table 1 lists the density of dangling bonds (db per area), as well as the surface energies of several different models calculated using the HOEP potential and DFT. The configurations have been listed in increasing order of the surface energies computed with HOEP, as this is the actual outcome of the global optimum searches. For reasons of space, we limit the number of structures in the Table 1 to at most six for each value of the relevant numbers of atoms in the simulation cell. However, when performing DFT relaxations we consider more structures than the ones shown in the table because we expect changes in their energetic ordering at the DFT level. The inclusion of a larger number of structures helps avoid excessive reliance on the empirical potential [12], which is mainly used a fast way to provide physically relevant reconstructions (i.e. where each atom at the surface has at most one dangling bond).

Table 1 and Fig. 1(b) suggest that the most unfavorable number of atoms in the simulation cell is $n = 215$, both at the level of HOEP and at the level of DFT. Therefore, it is justifiable to focus our attention on the other three values of n ($n = 216$, 214 and 213), which yield considerably lower surface energies. For each of these numbers of atoms, we present four low energy structures (as given by DFT), which are shown in Figs. 3–5. These structures are not necessarily the same as those enumerated in Table 1, as they are chosen based on their DFT surface energies. Since the global optimization has not been performed at the DFT level, the reader could argue that the lowest energy structure obtained after the sorting of the DFT-relaxed models may not be the DFT global minimum. While we found that a *thorough* sampling for systems with ~ 200 atoms is impractical at the DFT level, we have performed DFT relaxations for most of the local minima given by HOEP. Therefore, given the rather large set of structural candidates with different topological features considered here, the possibility of missing the actual reconstruction for Si(114) is much diminished in comparison with heuristic approaches.

We will now describe in turn the surface models corresponding to $n = 216$, 214 and 213. After the DFT relaxation, the lowest energy model that we found has turned out to be the same as the one proposed by Erwin and coworkers [5], perhaps with the exception of different relative tilting of the surface bonds. The model is shown in Fig. 3(a), and it

n	Bond counting $(db/3a^2\sqrt{2})$	HOEP (meV/Å^2)	DFT (meV/Å^2)
216	8	81.66	89.48
	8	83.16	90.34
	8	83.31	91.29
	8	83.39	88.77
	8	83.64	94.68
	8	84.42	92.16
215	8	91.61	97.53
	8	91.82	95.30
	8	92.00	94.20
	11	92.46	98.73
214	6	86.95	95.17
	10	87.32	99.58
	10	87.39	98.47
	10	87.49	93.88
	10	88.26	95.18
213	4	89.46	90.43
	6	89.76	94.01
	4	90.07	90.85
	6	91.73	94.66
	7	93.99	90.48

Table 1: Surface energies of different reconstructions for the Si(114) surface, sorted by the number of atoms n in the $3a \times a\sqrt{2}$ periodic cell. The second column shows the number of dangling bonds (counted for structures relaxed with HOEP) per unit area. The last two columns list the surface energies given by the HOEP interaction model [12] and by density functional calculations (DFT) [21] with the parameters described in text.

is characterized by the presence of dimers, rebonded atoms and tetramers occurring in this order along the (positive) [22$\bar{1}$] direction. These features have been well studied [5, 18], and we shall not insist on them here. The surface energy of the most stable model for Si(114)-(2) reconstruction is $\gamma = 88.77$ meV/Å^2. Although this surface energy is somewhat different from the previously reported value of 85 meV/Å^2 [5], the discrepancy between these absolute values can be attributed to the somewhat different computational parameters (slab thickness, number of k points) and/or different pseudopotentials.

It is notable that a different succession of the above-mentioned atomic scale features is also characterized by a low surface energy: specifically, dimers, tetramers and rebonded atoms (in this order along [22$\bar{1}$]), as shown in Fig. 3(c), give a surface energy which is only $\sim$2 meV/Å^2 higher than that of the Erwin *et al.* model shown in 3(a). This surface energy gap is apparently large enough to allow for another configuration [see Fig. 3(b)] with a surface energy that lies between the values corresponding to the first two models described above. As shown in Fig. 3(b), this new model has two consecutive dimer rows followed by a row of rebonded atoms, and arrangement that gives rise to surface corrugations of 0.4–0.5 nm. Remarkably, this corrugated model [Fig. 3(b)] is almost degenerate with the planar, (2×1) structure shown in Fig. 3(a). The last panel of Fig. 3 shows another planar model of Si(114), made of dimers, rebonded atoms and inverted tetramers, with the latter topological feature distinguishable as a seven-member ring when viewed along the [110] direction.

Dimers, rebonded atoms and tetramers also occur on low-energy structural models with $n = 214$, as shown in Fig. 4. The most favorable structure with $n = 214$ that we found [depicted in Fig. 4(a)] has a 5-coordinated subsurface atom and a 4-coordinated surface atom per unit cell. These topological features are determined by the bonding of a subsurface atom with one of the atoms of a tilted surface dimer; the corresponding surface energy is 90.09 meV/Å^2. Other structures with $n = 214$ atoms [examples shown in Fig. 4(b)–(d)] generally have higher energies than models with $n = 216$, (refer to Table 1) most likely because the two missing atoms lead to pronounced strains in the surface bonds.

The analysis of simulation slabs with $n = 213$ atoms reveals novel atomic scale features. Energetically favorable configurations with $n = 213$ [5(a) and (c)] show a 5-atom ring on the surface stabilized by a subsurface interstitial, a structural complex that was first encountered in the case of Si(113) surface [2]. Structures in Figs. 5(a) and (c) differ in terms of the succession of the topological features along the [22$\bar{1}$] direction, i.e. dimers, 5-member rings, rebonded atoms [5(a)] as opposed to dimers, rebonded atoms and 5-member rings [5(c)]. The model in Fig. 5(a) is degenerate with the one shown in 5(b), as their relative surface energy is much smaller than the 1–2 meV/Å^2 expected accuracy of the relative surface energies determined here. The reconstruction 5(b) is very similar to the lowest energy structure in Fig. 3(a) (achievable with $n = 212$): the only different feature is the extra atom lying in between two rebonded atoms and sticking out of the surface [refer to Fig. 5(b)]. Likewise, the model in Fig. 5(d) can be obtained from structure 3(b) by adding one atom per unit cell in such a way that it bridges the two atoms of a dimer on one side, and rebonds on the other

side.

3.2 Discussion

The data in Table 1 shows clearly that the density of dangling bonds at the Si(114) surface is, in fact uncorrelated with the surface energy. The lowest number of dbs per area reported here is 4, and it corresponds to $n = 213$ and $\gamma = 90.43$ meV/Å^2 at the DFT level. The optimum structure [3(a)] , however, has twice as many dangling bonds but the surface energy is smaller, 88.77 meV/Å^2. Furthermore, for the same number of atoms in the supercell ($n = 216$) and the same dangling bond density ($8db/3a^2\sqrt{2}$), the different reconstructions obtained via global searches span an energy interval of at least 5 meV/Å^2. These findings constitute a clear example that the number of dangling bonds can not be used as a criterion for selecting model reconstructions for Si(114); we expect this conclusion to hold for many other high-index semiconductor surfaces as well.

The HOEP surface energy and the DFT surface energy also show very little correlation, indicating that the transferability of the interaction model [12] for Si(114) is not as good as, for instance, in the case of Si(001) and Si(105) [6]. The most that can be asked from this model potential [12] is that the observed reconstruction [5] is amongst the lower lying energetic configurations –which, in this case it is. We have also tested the transferability of HOEP for the case of Si(113), and found that, although the ad-atom interstitial models [2] are not the most stable structures, they are still retrieved by HOEP as local minima of the surface energy. We found that the low-index (but much more complex) Si(111)-(7×7) reconstruction is also a local minimum of the HOEP interaction model, albeit with a very high surface energy. Other tests indicated that, while the transferability of HOEP to the Si(114) orientation is marginal in terms of sorting structural models by their surface energy, this potential [12] performs much better than the more popular interaction models [17, 24], which sometimes do not retrieve the correct reconstructions even as local minima. Therefore, HOEP is very useful as a way to find different local minimum configurations for further optimization at the level of electronic structure calculations.

A practical issue that arises when carrying out the global searches for surface reconstructions is the two-dimensional periodicity of the computational slab. In general, if a periodic surface pattern has been observed, then the lengths and directions of the surface unit vectors may be determined accurately through experimental means (e.g., STM or LEED analysis): in those cases, the periodic vectors of the simulation slab should simply be chosen the same as the ones found in experiments. When the surface does not have two-dimensional periodicity, or when experimental data is difficult to analyze, then one should systematically test computational cells with periodic vectors that are integer multiples of the unit vectors of the bulk truncated surface, which are easily computed from knowledge of crystal structure and surface orientation. There is no preset criterion as to when the incremental testing of the size of the surface cell should be stopped –other than the limitation imposed by finite computational resources; nevertheless, this approach gives a systematic way of ranking the surface energies
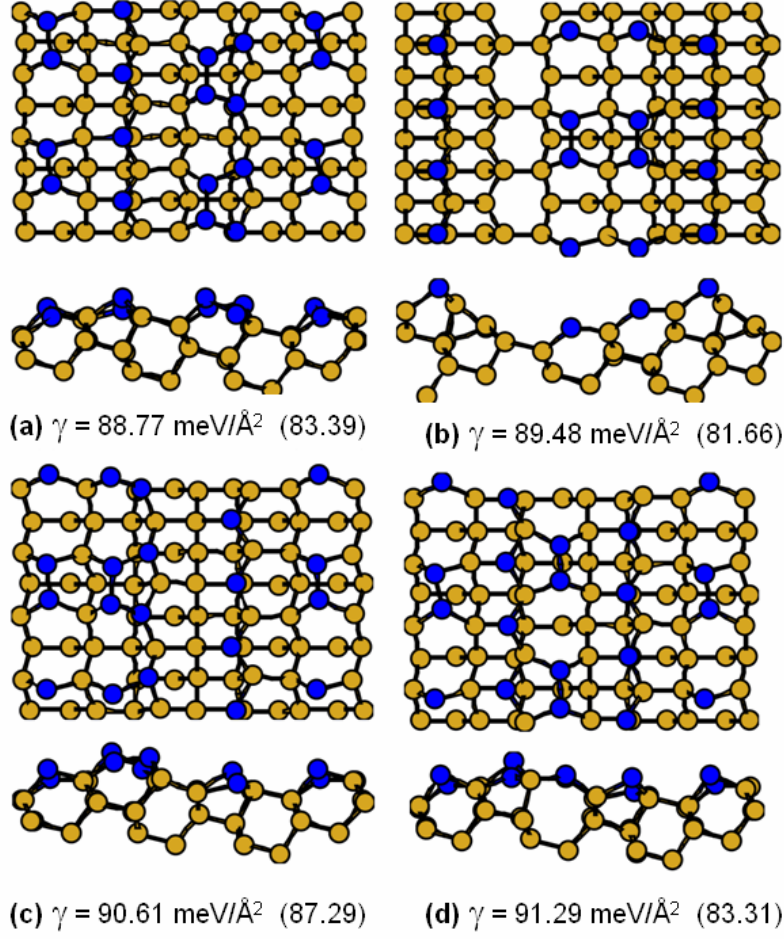
(a) $\gamma = 88.77$ meV/Å² (83.39)

(b) $\gamma = 89.48$ meV/Å² (81.66)

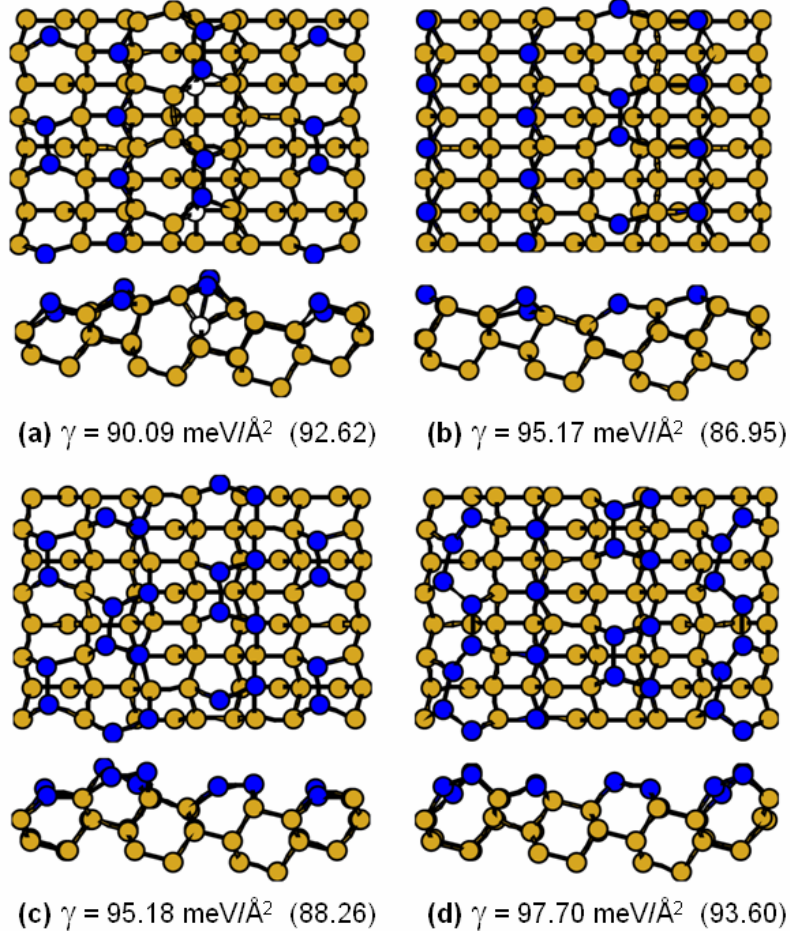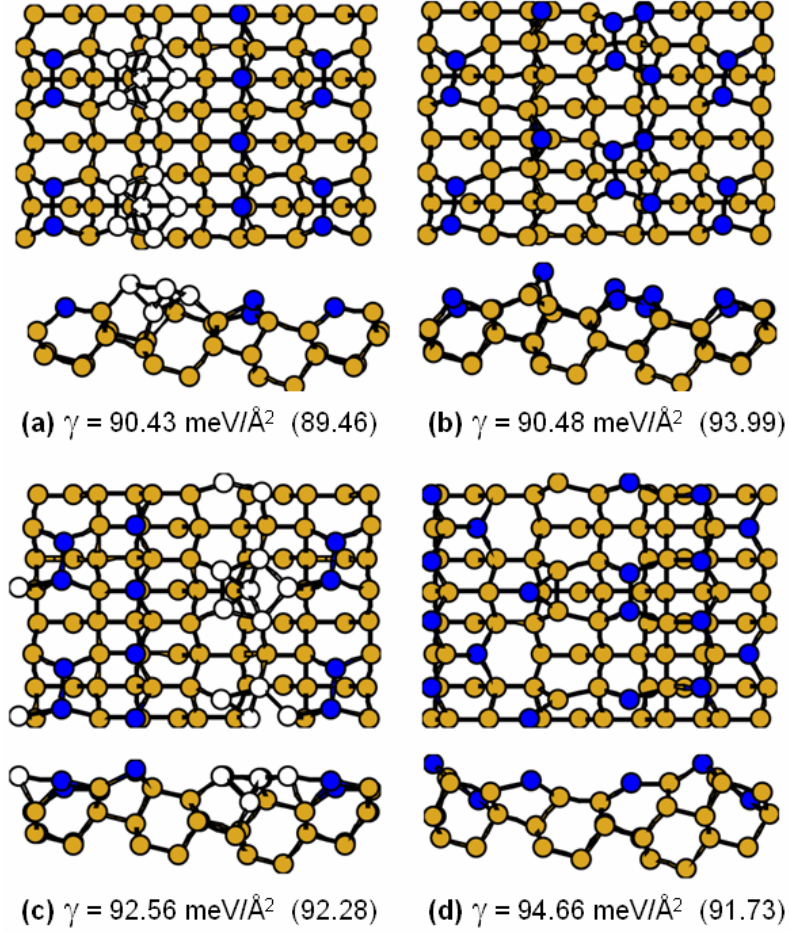(c) $\gamma = 90.61$ meV/Å² (87.29)

(d) $\gamma = 91.29$ meV/Å² (83.31)

Figure 3: Structural models (top and side views) of Si(114)-(2×1), with $n = 216$ atoms per unit cell after relaxation with density functional methods [21]. The surface energy γ computed from first-principles is indicated for each structure, along with the corresponding value (in parentheses) obtained using the empirical potential [12]. The darker shade marks the undercoordinated atoms.

14

(a) $\gamma = 90.09$ meV/Å^2 (92.62) **(b)** $\gamma = 95.17$ meV/Å^2 (86.95)

(c) $\gamma = 95.18$ meV/Å^2 (88.26) **(d)** $\gamma = 97.70$ meV/Å^2 (93.60)

Figure 4: Structural models (top and side views) of Si(114)-(2×1), with $n = 214$ atoms per unit cell after relaxation with density functional methods [21]. The surface energy γ computed from first-principles is indicated for each structure, along with the corresponding value (in parentheses) obtained using the empirical potential [12]. The darker shade marks the undercoordinated atoms, while the overcoordinated atoms are shown in white.

Figure 5: Structural models (top and side views) of Si(114)-(2×1), with $n = 213$ atoms per unit cell after relaxation with density functional methods [21]. The surface energy γ computed from first-principles is indicated for each structure, along with the corresponding value (in parentheses) obtained using the empirical potential [12]. The darker shade marks the under-coordinated atoms, while the white atoms are either four-coordinated or overcoordinated.

of slabs of different areas, and eventually finding the global minimum surface structure.

Motivated by a previous finding that larger unit cells can lead to models with very low surface energies (see, for instance the example of Si(105) [6, 7]), we have also performed global minimum search using GA for slabs of dimensions $6a \times a\sqrt{2}$, which correspond to a doubling of the unit cell in the $[22\bar{1}]$ direction. The ground state structure at the HOEP level found in this case is still the corrugated model 3(b) with a surface energy of $\gamma = 81.66$ meV/Å^2. As a low-lying configuration we again retrieve the original model [5] with $\gamma = 83.39$ meV/Å^2. Furthermore, we also find a several models that have surface energy in between the two values, characterized by the presence of different $3a \times a\sqrt{2}$ structures in the two halves of the $6a \times a\sqrt{2}$ simulation cell. This finding suggests that $[1\bar{1}0]$-oriented boundaries between different $3a \times a\sqrt{2}$ models on Si(114) are not energetically very costly: this is consistent with the experimental reports of Erwin *et al.*, who indeed found (2×1) and $c(2 \times 2)$ structures next to one another [5].

4 Concluding remarks

In conclusion, we have obtained and classified structural candidates for the Si(114) surface reconstructions using global optimization methods and density functional calculations. We have used both parallel-tempering Monte Carlo procedure coupled with an exponential cooling [6], as well as the genetic algorithm [7]. Both of the methods are used in conjunction with the latest empirical potential for silicon [12], which has a better transferability in comparison with more popular potentials [17, 24]. We have built a large database of structures (reported, in part, in Table 1) which were further optimized at the DFT level. The lowest energy structure that we found (Fig. 3(a)) after the DFT relaxation is the same as the one originally reported for Si(114)-(2×1) in [5].

In addition, we have discovered several other types of structures (refer to Figs. 3(b), 3(c) and 4(a) and 5(a)) that are separated (energetically) by 1–2 meV/Å^2 from the lowest energy model [5]. Given that the relative surface energies at the DFT level have an error of ± 1 meV/Å^2, and that the experiments of Erwin *et al.* [5] already identified two reconstructions ($[(2 \times 1)$ and $c(2 \times 2)]$ whose surface energies are within 1–2 meV/Å^2 from one another, it is conceivable that some of the models in Figs. 3–5 could also be found on the Si(114) surface. This prediction could be tested, e.g., by high-resolution transmission electron microscopy experiments such as the ones reported recently for the Si(5512) surface [25]. Low-energy electron diffraction experiments, as well as more STM measurements could also shed light on whether there exist other structural models on a clean Si(114) surface than initially reported in Ref. [5].

References

[1] D. P. Woodruff, Surf. Sci. **500**, 147 (2002).

[2] J. Dąbrowski, H. J. Müssig, G. Wolff, Phys. Rev. Lett. **73**, 1660 (1994).

[3] A. A. Baski, S. C. Erwin, L. J. Whitman, Science **269**, 1556 (1995).

[4] Y. W. Mo, D. E. Savage, B. S. Swartzentruber, M. G. Lagally, Phys. Rev. Lett. **65**, 1020 (1990).

[5] S. C. Erwin, A. A. Baski, L. J. Whitman, Phys. Rev. Lett. **77**, 687 (1996).

[6] C. V. Ciobanu and C. Predescu, Phys. Rev. B **70**, 085321 (2004).

[7] F. C. Chuang, C. V. Ciobanu, V. B. Shenoy, C. Z. Wang, K. M. Ho, *Finding the reconstruction of semiconductor surfaces via a genetic algorithm*, Surf. Sci. Lett. (in press).

[8] F. H. Stillinger and T. A. Weber, Phys. Rev. A **28**, 2408 (1983).

[9] F. H. Stillinger, Phys. Rev. E **59**, 48 (1999).

[10] C. J. Geyer and E. A. Thompson, J. Am. Stat. Assoc. **90**, 909 (1995).

[11] K. Hukushima and K. Nemoto, J. Phys. Soc. Jpn. **65**, 1604 (1996).

[12] T. J. Lenosky, B. Sadigh, E. Alonso, V. V. Bulatov, T. Diaz de la Rubia, J. Kim, A. F. Voter, and J. D. Kress, Modelling Simul. Mater. Sci. Eng. **8**, 825 (2000).

[13] N. Metropolis, A. W. Rosenbluth, M. N. Rosenbluth, A. M. Teller, E. Teller, J. Chem. Phys. **21**, 1087 (1953).

[14] U. H. E. Hansmann, Chem. Phys. Lett **281**, 140 (1997).

[15] Y. Sugita, A. Kitao, and Y. Okamoto, J. Chem. Phys. **113**, 6042 (2000).

[16] C. Predescu, M. Predescu, and C. V. Ciobanu, J. Chem Phys. **120**, 4119 (2004).

[17] F. H. Stillinger and T. A. Weber, Phys. Rev. B **31**, 5262 (1985).

[18] R. D. Smardon, G. P. Srivastava, S. J. Jenkins, Phys. Rev. B **69**, 085303 (2004); R. D. Smardon, G. P. Srivastava, Surf. Sci. **566-568**, 895 (2004).

[19] D. M. Deaven and K. M. Ho, Phys. Rev. Lett. **75**, 288 (1995).

[20] K. M. Ho, A. A. Shvartsburg, B. C. Pan, Z. Y. Lu, C. Z. Wang, J. Wacker, J. L. Fye, and M. F. Jarrold, Nature **392**, 582 (1998).

[21] S. Baroni, A. Dal Corso, S. de Gironcoli, and P. Giannozzi, http://www.pwscf.org.

[22] J.P. Perdew and A. Zunger, Phys. Rev. B **23**, 5048 (1981).

[23] A. A. Baski, S. C. Erwin, L. J. Whitman, Surf. Sci. **392**, 69 (1997).

[24] J. Tersoff, Phys. Rev. B **38**, 9902 (1988);*ibid* Phys. Rev. B **37**, 6991 (1988).

[25] J. Liu, M. Takeguchi, M. Tanaka, H. Yasuda, K. Furuya, J. Electron Microsc. **50**, 541 (2001).